Electronic Supplementary Material (ESI) for ChemComm.

Electronic Supplementary Information

Coordination-induced gelation of an L-glutamic acid Schiff base derivative: the anion Hofmeister effect and cyanide-specific selectivity

Jinguo Sun‡, Yucun Liu‡, Longyi Jin, Tie Chen* and Bingzhu Yin*

Key Laboratory of Natural Resources of Changbai Mountain & Functional Molecules of Ministry of Education, Department of Chemisrey, Yanbian University, Yanji, Jilin 133002, PR China.
E-mail: zqcong@ybu.edu.cn;
Fax: +86 433 2732456;
Tel: +86 433 2732298.

1. Instrumentation

Gelation study

A weight amount of molecule **G** with metals adding a measured volume of the solvent were placed in a sealed test tube and made a clear solution by heating. And then, the system left at room temperature. The transition temperatures (T_{gel}) were determined by ball-drop method.

NMR experiments

All solution state NMR studies were carried out on Bruker AV-300 Spectrometer (300 MHz for ^{1}H and 75 MHz for ^{13}C) and chemical shifts were referenced relative to tetramethylsilane (δ_H/δ_C=0).

FT-IR spectroscopy

IR spectra were recorded on a Shimadzu FT-IR Prestige-21 instrument with the KBr disk technique.

MALDI-TOF-MS spectrometry and High-resolution mass spectra (HRMS)

Mass spectra were performed on a Shimadzu Axima CFR^{TM} Plus using a 1,8,9-anthracenetriol (DITH) and β-phenylacrylic acid (CHCA) matrix.
High-resolution mass spectra (HRMS) were obtained using a Bruker microTOF II focus spectrometer (ESI).

Circular dichroism (CD) spectroscopy

CD spectra were obtained on Chirascan spectrometer using a 1 mm path-length cell.

Atomic force microscopy (AFM)

For AFM experiments, 10 µL of sample solution (diluted gels) was drop-casted onto a freshly cleaved mica surface. Each sample was air-dried 48 h in a dust-free environment prior to AFM imaging. The images were obtained by scanning the mica surfaces in air under ambient conditions using Agilent-5500 in tapping mode.

UV-vis spectroscopy

UV-vis spectra were recorded on a Hitachi U-3010 spectrophotometer.

Fluorescence spectroscopy

Fluorescence spectra were recorded on a Shimadzu RF-5301PC fluorescence spectrophotometer.

Field emission scanning electron microscopy

The gel samples were placed on silicon wafer, and dried for 24h under room temperature before imaging. A layer of gold was sputtered on top to form a conducting surface and finally the specimen was transferred into the Field Emission Scanning Electron Microscope (FE-SEM, Joel Scanning Microscope-JSM-6700F).

X-ray scattering

Small-angle X-ray scattering (SAXS) measurements were carried out at 298 K on a beamline 1W2A synchrotron radiation X-ray small angle system at Beijing Synchrotron Radiation Facility(λ =1.54Å) and wide -angle X-ray diffracting (WAXRD) measurements were carried out at 298 K on the glass-sustained xerogel films and recorded on a Bruker D8/ADVANCE X-ray diffractmeter (Germany) with radiation (λ =1.54Å).

2. Synthesis and characterization of organic compounds

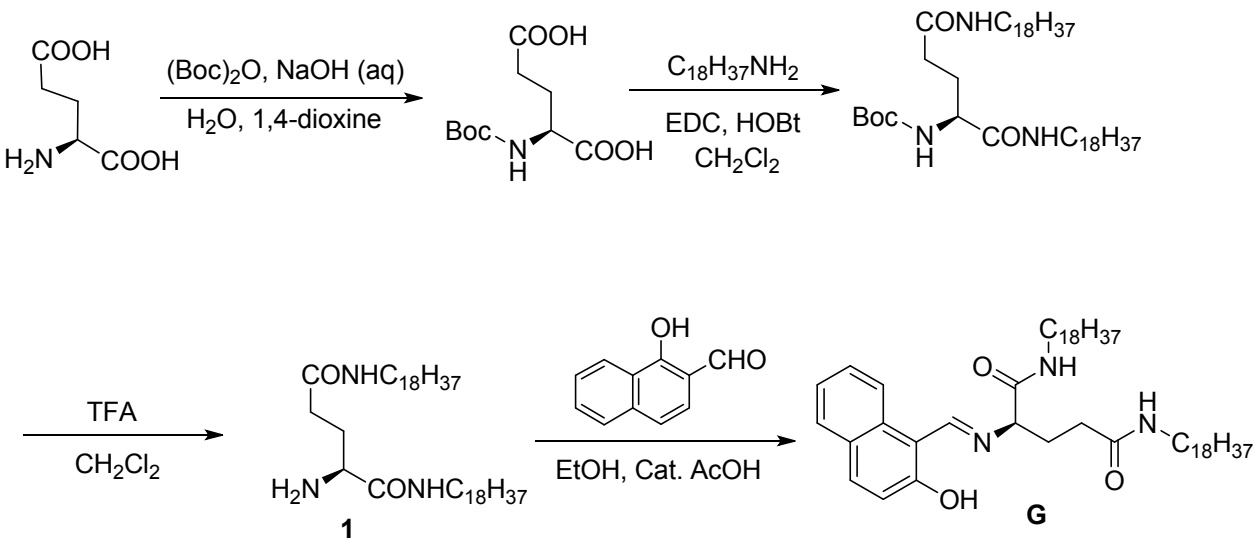

Scheme S1. The synthetic route of compound G.

Compounds **1** were synthesized according to literatures methods.[1]

Compound **G** was synthesized as follow: 2-hydrox-1-naphthaldehyde (1 mmol), compound **1** (1 mmol) and acetic acid (40 μL, as a catalyst) were added to ethanol (10 mL). Then the reaction mixture was stirred under refluxed conditions for 6 hours, the crude solutions were cooled and filtered. The filtered powder was recrystallized with C_2H_5OH to get solid of compound **G**. yellow powder, Yield: 80%. Characterization of **G**: m.p. 130-131 ^oC. ^1H NMR ($CDCl_3$, 300 MHz): δ, 14.2 (br, 1H, OH), 9.31 (s, 1H, -N=CH-), 8.04 (d, *J* = 7.8 Hz, 1H, ArH), 7.82(d, *J* = 9.0 Hz, 1H, ArH), 7.74 (d, *J* = 7.8 Hz, 1H, ArH), 7.54 (t, *J* = 7.2 Hz, 1H, ArH), 7.35 (t, *J* = 7.2 Hz, 1H, ArH), 7.10 (d, *J* = 9.0 Hz, 1H, -ArH), 6.28 (s, 1H, -NH), 5.83 (s, -NH), 4.18 (s, 1H, CH), 3.18-3.34 (m, 4H), 2.20-2.41 (m, 4H), 1.42-1.53 (m, 4H), 1.20-1.29 (m, 60H), 0.88 (t, *J* = 6.6 Hz, 6H) ppm. ^{13}C NMR ($CDCl_3$, 300 MHz): 171.71, 170.20, 162.16, 136.16, 132.94, 127.32, 123.60, 121.13, 119.05, 108.19, 69.79, 39.69, 31.94, 30.85, 29.90, 26.90, 22.71, 14.15 ppm. IR (KBr, cm-1) *v*: 3315 (OH), 3093 (NH), 3049 (NH), 1619(C=O). MALDI-TOF-MS calcd for $C_{52}H_{89}N_3O_3$: 804.28; found: 805.7 $[M+H]^+$.

Reference

[1] Y. G. Li, T. Y. Wang and M. H. Liu, Soft Matter, 2007, 3, 1312.

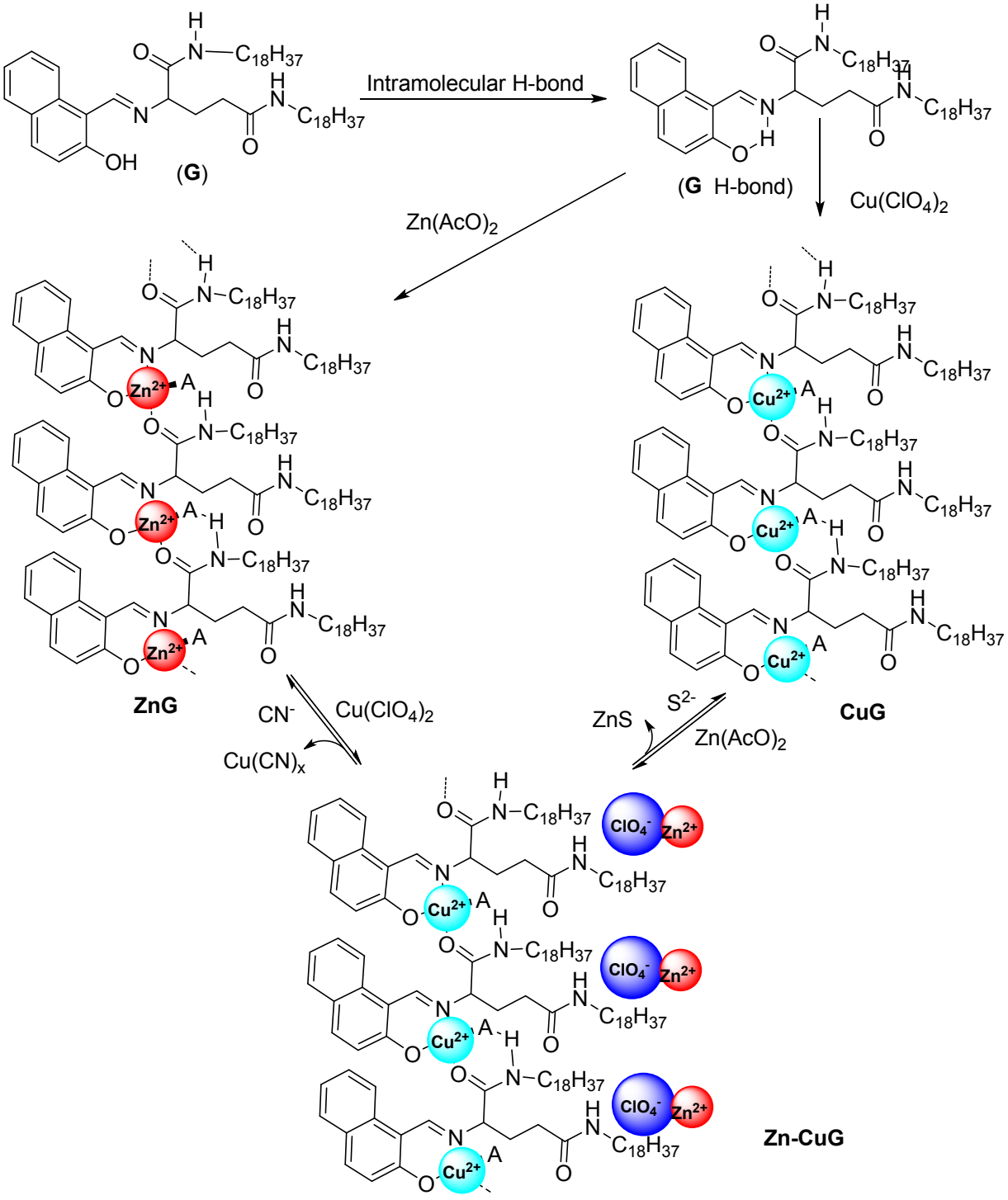

Scheme S2 Chemical structure of the **G** and the assumed self-assembly and stimuli-responsive mechanism.

Table S1 Gelation Properties of **G, ZnG, CuG** and **Zn-CuG**.

Solvents	**G**	**ZnG**	**CuG**	**Zn-CuG**
	Phases			
Cyclohexane	P[a]	P	P	P
Toluene	P	P	P	P
Petroleum ether	P	P	P	P
THF	S	S	S	S
Chloroform	S	S	S	S
Dichloromethane	S	S	S	S
Acetone	P	P	P	P
Acetonitrile	P	P	P	P
DMF	P	S	1.0 % (TG)	S
DMSO	P	0.93%[b] (TG)	0.88 % (TG)	1.0 % (TG)
Methanol	P	P	P	P
Ethanol	P	P	P	P
Glycol	P	S	S	S
Propyl alcohol	P	S	P	P
Isopropanol	P	P	P	P
Benzene	P	P	P	P
Benzyl acohol	S	S	S	S
Chlorobenzene	S	P	P	P
Ethyl acetate	P	P	P	P
n-hexane	P	P	P	P

[a]TG: transparent gel; S: solution; P: precipitation

[b]The critical gelation concentration (wt %, 10 mg/mL = 1%).

2. Figures

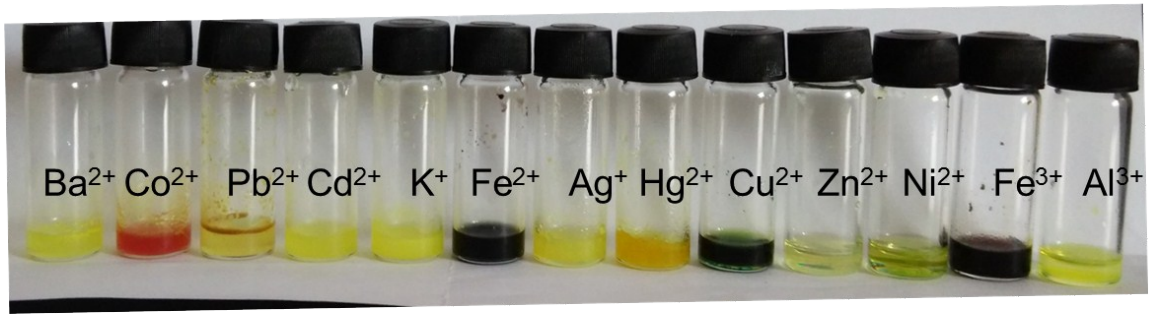

Fig. S1 Photographs of the solutions of **G** in DMSO (10 mg/mL) in the presence of one equiv. of various metal ions as their perchlorate salts.

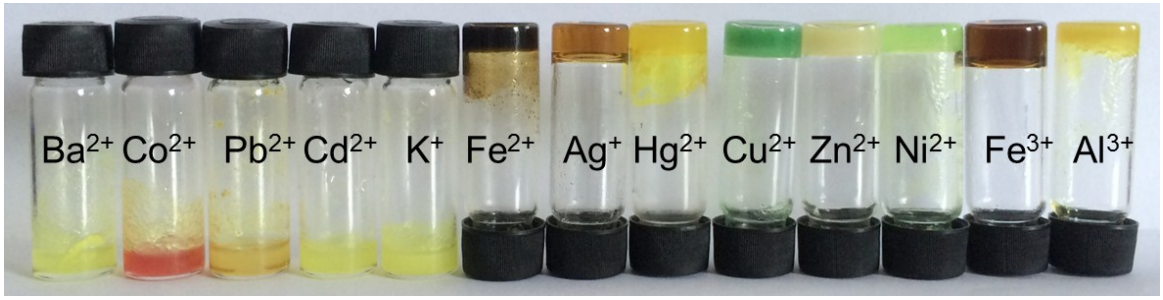

Fig. S2 Photographs of the solutions or gels of **G** and cation in DMSO (**G**: 10 mg/mL) in the presence of sodium acetate (**G**: cation: sodium acetate =1: 1: 1).

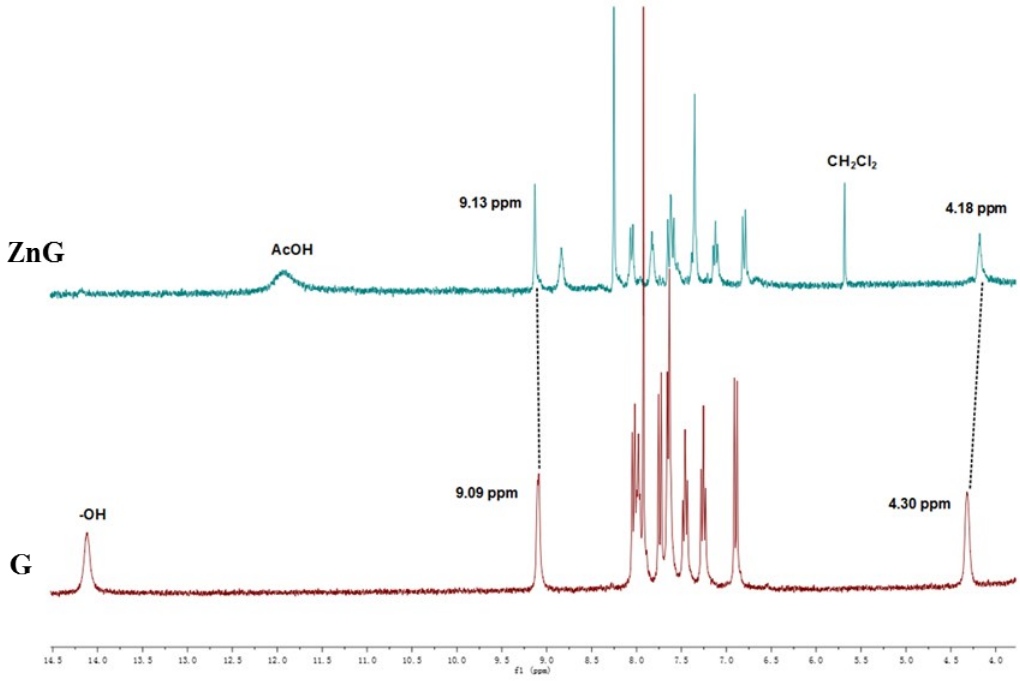

Fig. S3 Partial ^{1}H NMR spectra of **G** and **ZnG** in d_6-DMSO-$CDCl_3$ (v/v, 5:2)

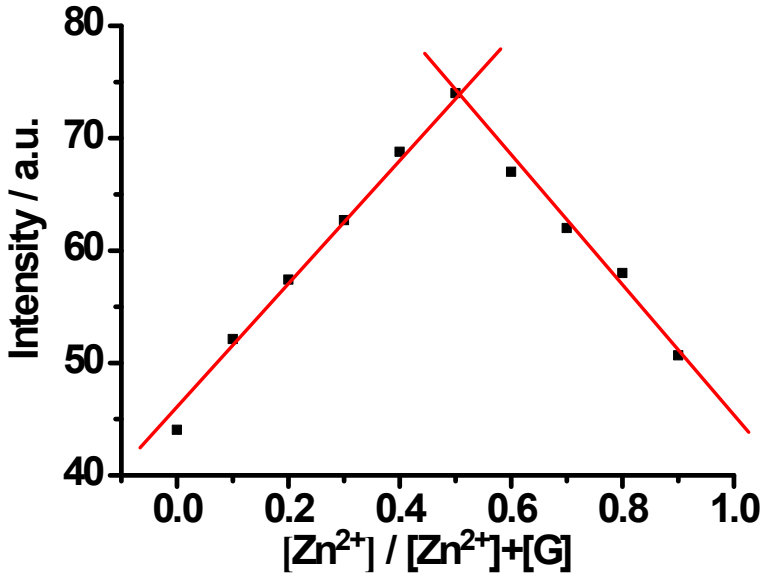

Fig. S4 Job's plot between **G** and Zn^{2+} based on the data of fluorescence spectra. [**G**] + [Zn^{2+}]= 1 μM.

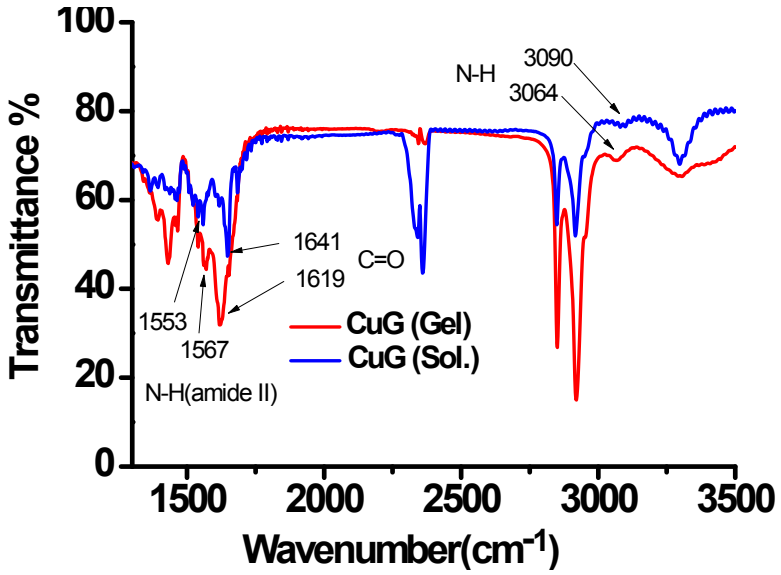

Fig. S5 FT-IR spectra of solution and xerogel of metallogel **ZnG** (obtained from 1 % DMSO metallogel, **ZnG**, **G** : Zn^{2+} = 1 : 1).

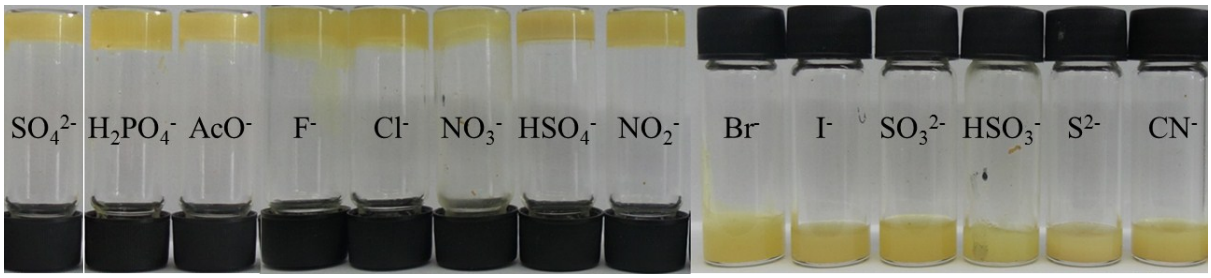

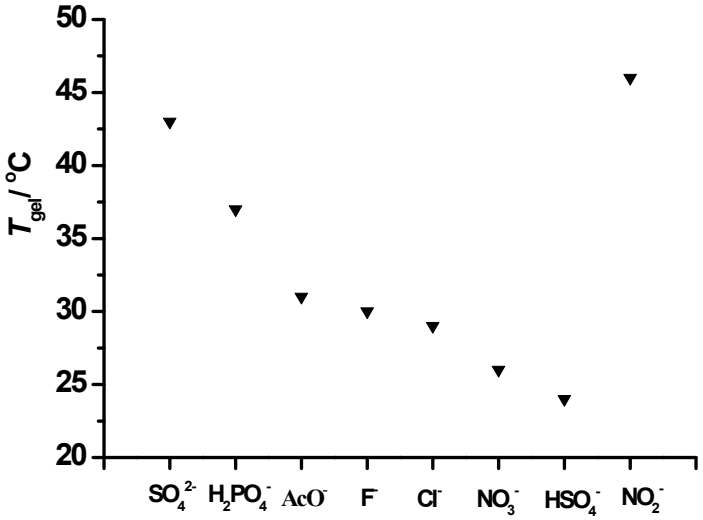

Fig. S6 Photograph of solutions and gels of **G** and $Zn(ClO_4)_2$ in DMSO (**G**: 10mg/mL) in the presence of various anions (**G** : anion: Zinc perchlorate =1 : 1: 1, up) and melting temperature (T_{gel}) of the gels of G and Zn^{2+} in presence of various anions in DMSO (down).

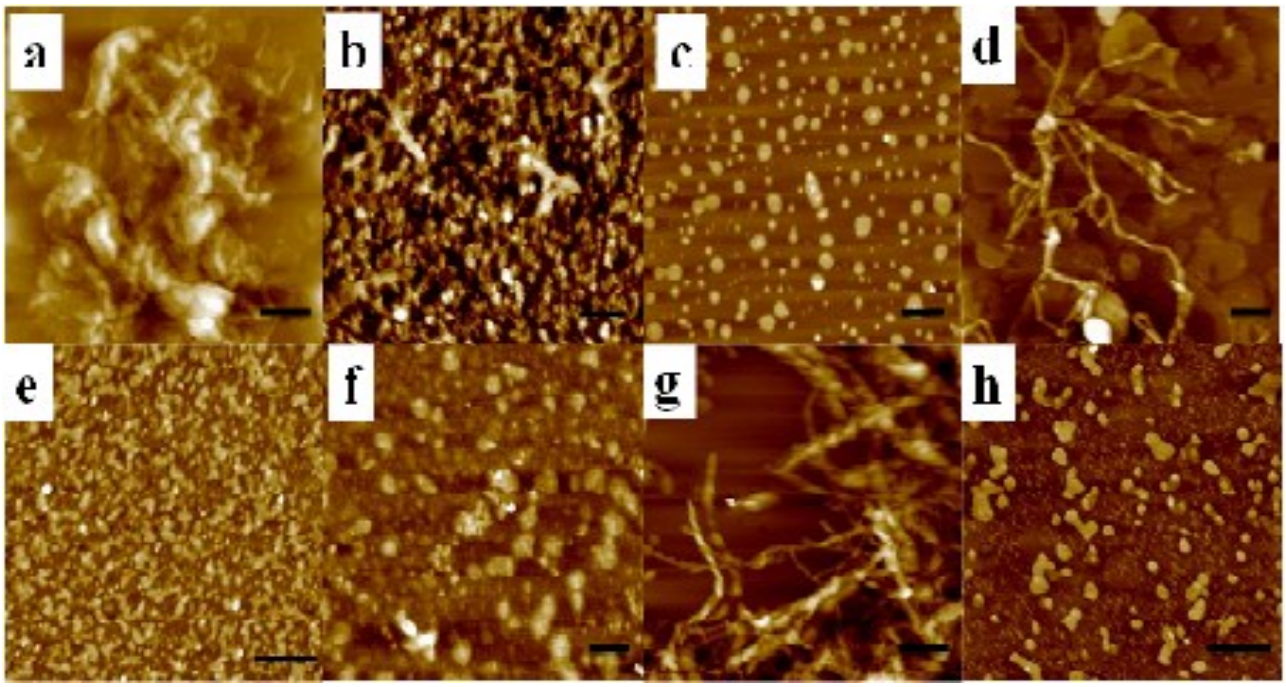

Fig. S7 AFM images of metallogels **CuG**. Counterions: a) sulfate, b) phosphate, c) acetate, d) fluoride, e) chloride, f) nitrate, g) bisulfate and h) nitrite salts of sodium. Scale bar represents 500 nm.

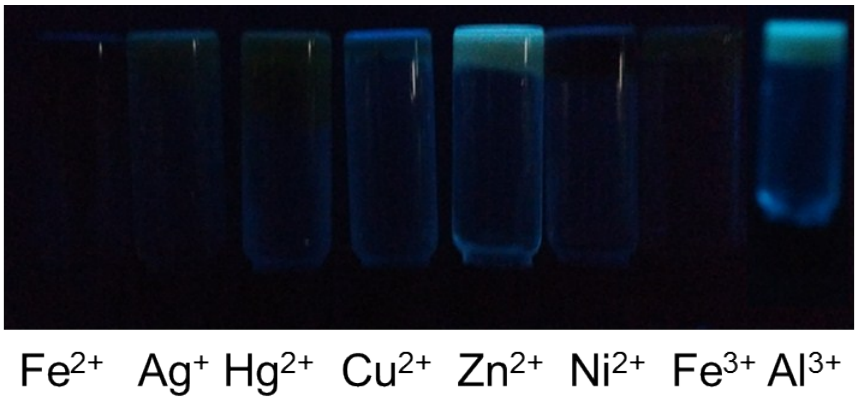

Fig. S8 Photographs of gels of compound **G** and $Cu(ClO_4)_2$ in DMSO (**G**: 10 mg/mL) in the presence of various metal ions as their acetates (**G**: cation: sodium acetate =1: 1: 1) under UV light.

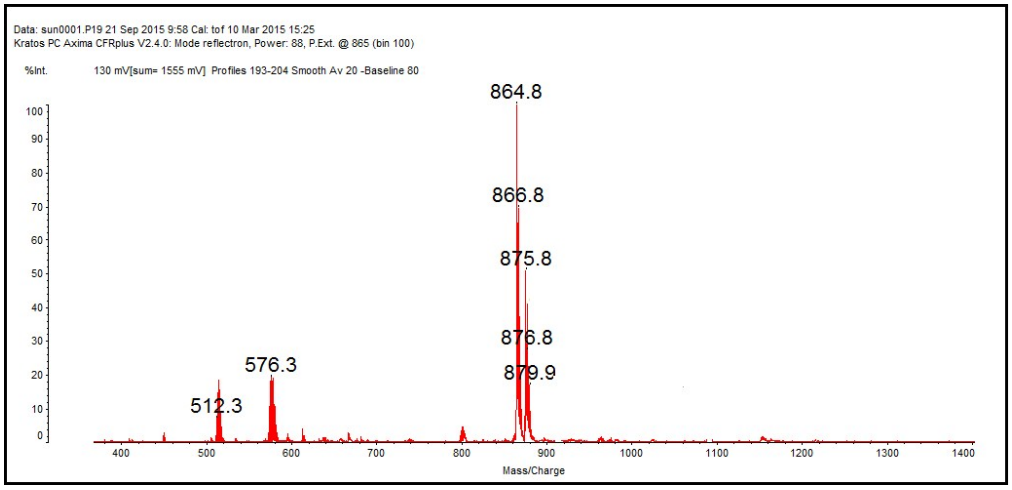

Fig. S9 MAFDI-TOF-MS of **Zn-CuG**.

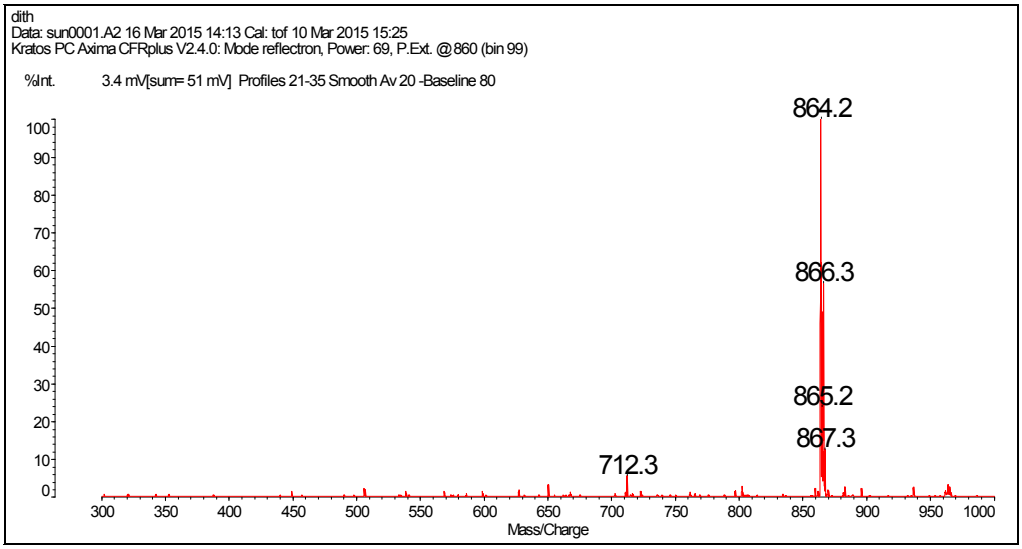

Fig. S10 MAFDI-TOF-MS of **CuG**.

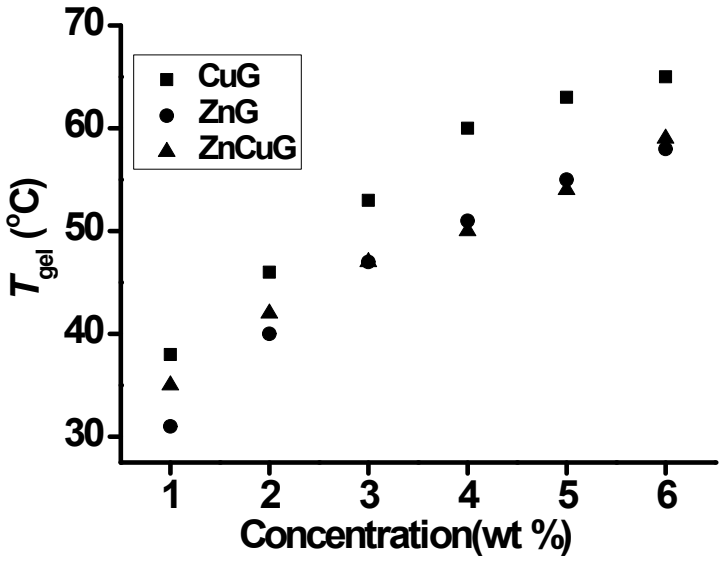

Fig. S11 Plots of T_{gel} against the concentrations of metalogels ZnG, **CuG** and **Zn-CuG** from DMSO (for **ZnG**, **G** : Zn^{2+} = 1 : 1; for **CuG**, Cu^{2+} : **G**=1:1; for **Zn-CuG**, **G** :Cu^{2+} : Zn^{2+} =1:1:1).

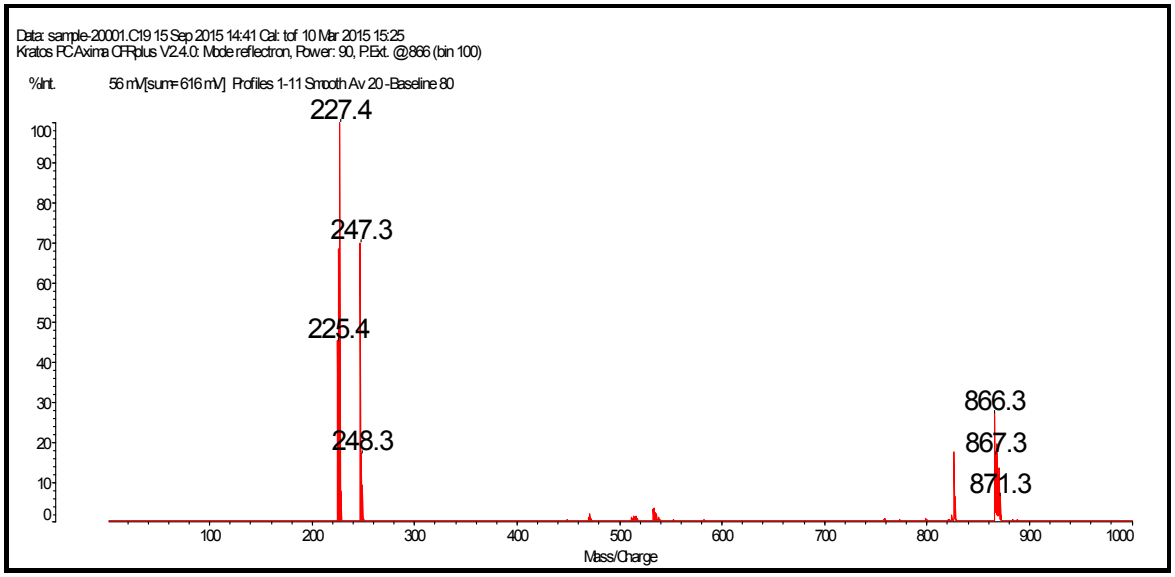

Fig. S12 MAFDI-TOF-MS of **Zn-CuG** treated with CN^- (2 equiv.). [G + Zn^{2+} - H] = 866.61, found 866.3.

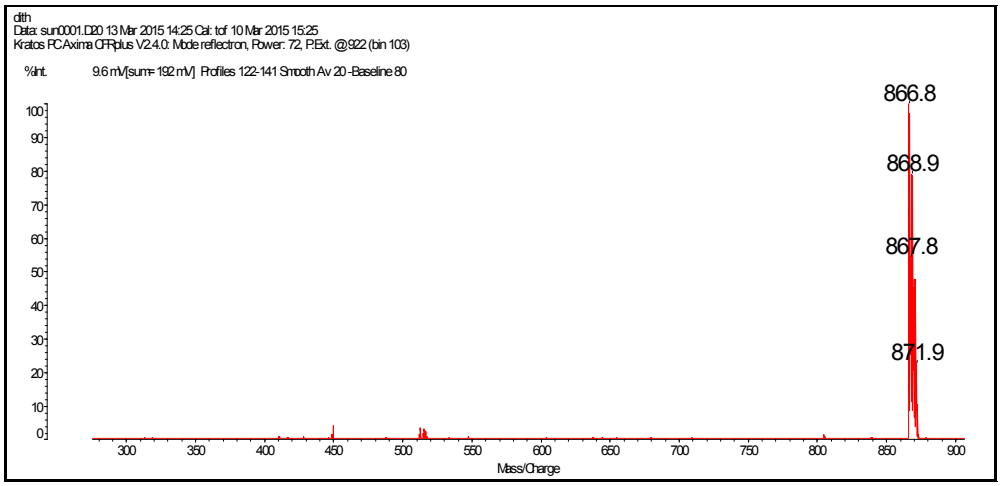

Fig. S13 MAFDI-TOF-MS of **ZnG.** [G + Zn^{2+} - H] = 866.61, found 866.8.

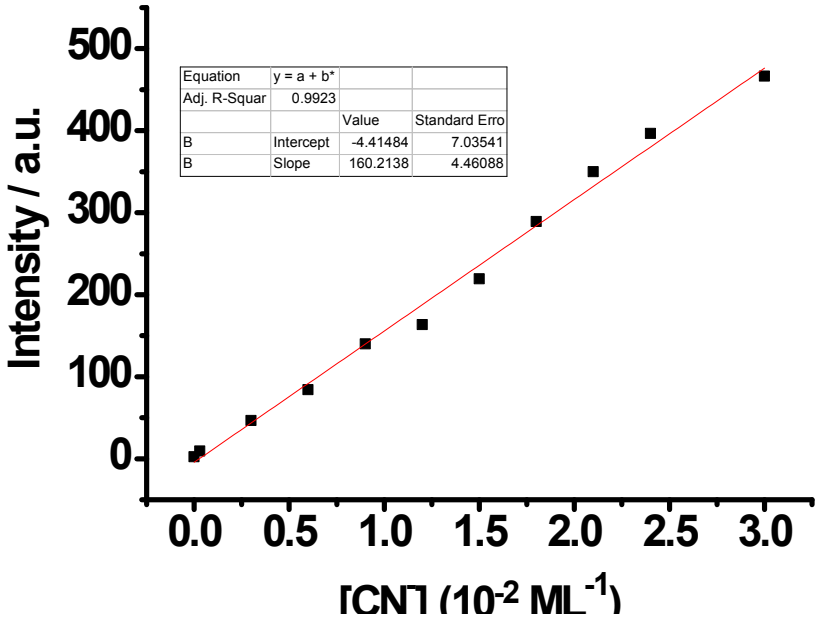

Fig. S14 Plot of the emission intensities of **Zn-CuG** at 457 nm as a function for concentrations of CN^-.

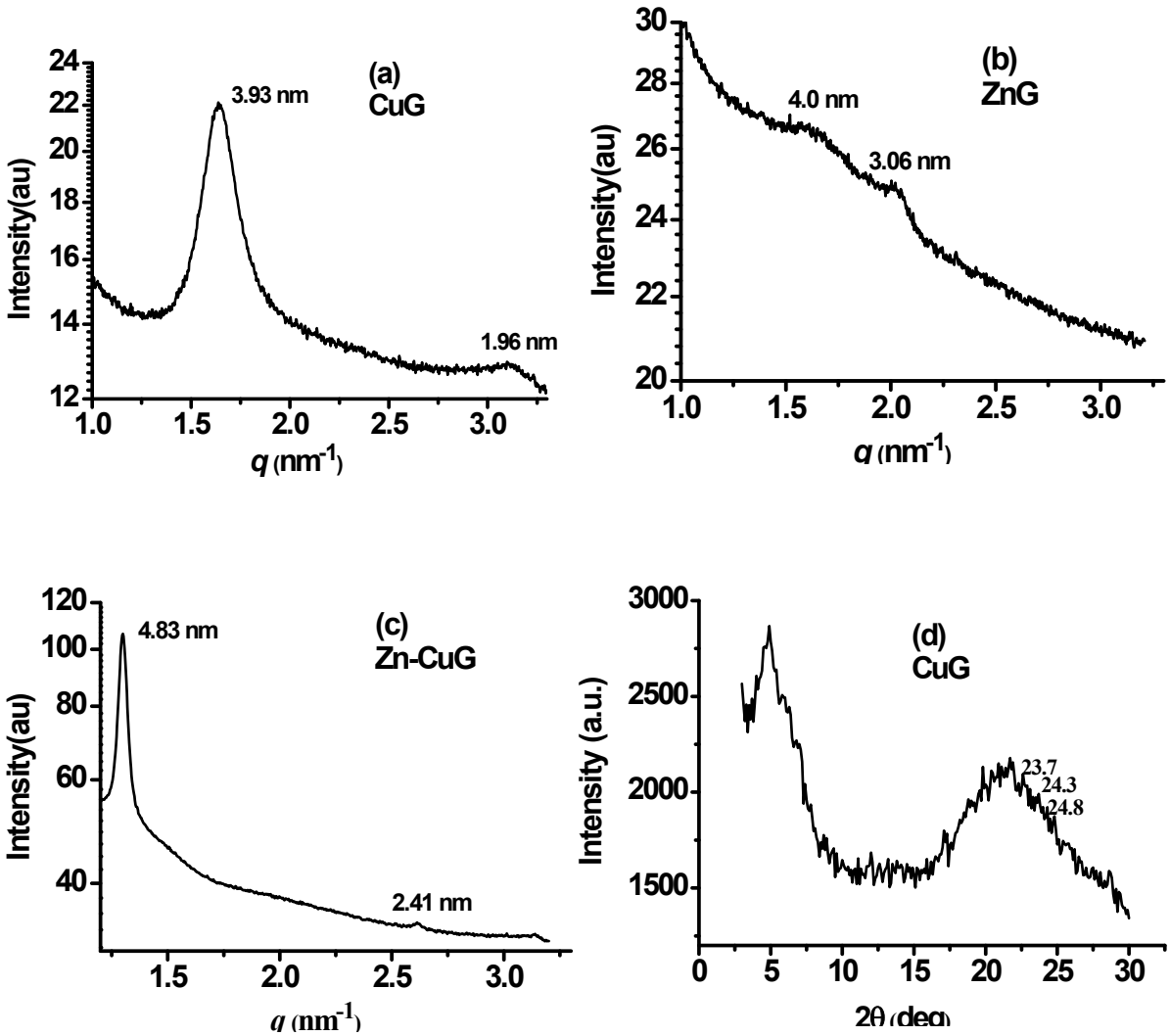

Fig. S15 Powder SXRD and WXRD patterns of xerogels of **CuG** (a), **ZnG** (b), (c) **Zn-CuG** and (d) **CuG**, respectively (obtained from 1% DMSO solutions of metallogels; for **CuG**, G : Cu^{2+} = 1 : 1; for **ZnG**, G : Zn^{2+} = 1 : 1); for **ZnCuG**, G : Cu^{2+} : Zn^{2+} = 1 : 1 : 1).

To gain further insight into the structures of the metallogels, small angle X-ray diffraction (SAXRD) measurements were performed. As shown in Figure S12a, the reflection peaks of **CuG** corresponding to *d*-spacing of 3.93 and 1.96 nm were detected following the ratio of 1 : ½, which revealing the lamellar structure of the supramolecular gel. The calculated length of compound **1** molecule was 3.21 nm (CPK space-filling model), indicating that the space lattice was composed of two molecules with the flexible chains interdigitated or Inclined. As for the xerogel of **ZnG**, the diffraction peaks appeared at *q* values of 1.57 and 2.05 nm^{-1}, respectively, following the ratio of 1: √2. It strongly reveals the rectangular columnar structure of the **ZnG** with a = 4 nm and b = 4.05 nm (Figure S12b). The number of molecules within the cell unit was approximately 12 with two molecules cross together based on calculations using the equation. When doped Cu^{2+} into the **ZnG**, the bilayer lamellar structure was formed in the **Zn-CuG** system, with a scattering vector ratio of 1:2 (*q* values were 1.3 and 2.6 nm^{-1}). However, the layer distance of the **Zn-CuG** was estimated to be 4.83 nm which was larger than interlayer spacing of the **CuG** (Figure S12c). Moreover, the peaks at

2θ = 21.9–24.8° corresponded to *d*-spacing 3.58–4.05 Å**,** which suggested that π–π stacking existed in the naphthyl and alkyl groups of these gels (Figure S12d). The reasonable packing of the metallogels in the aggregates in DMSO is schematically represented in Figure S13.

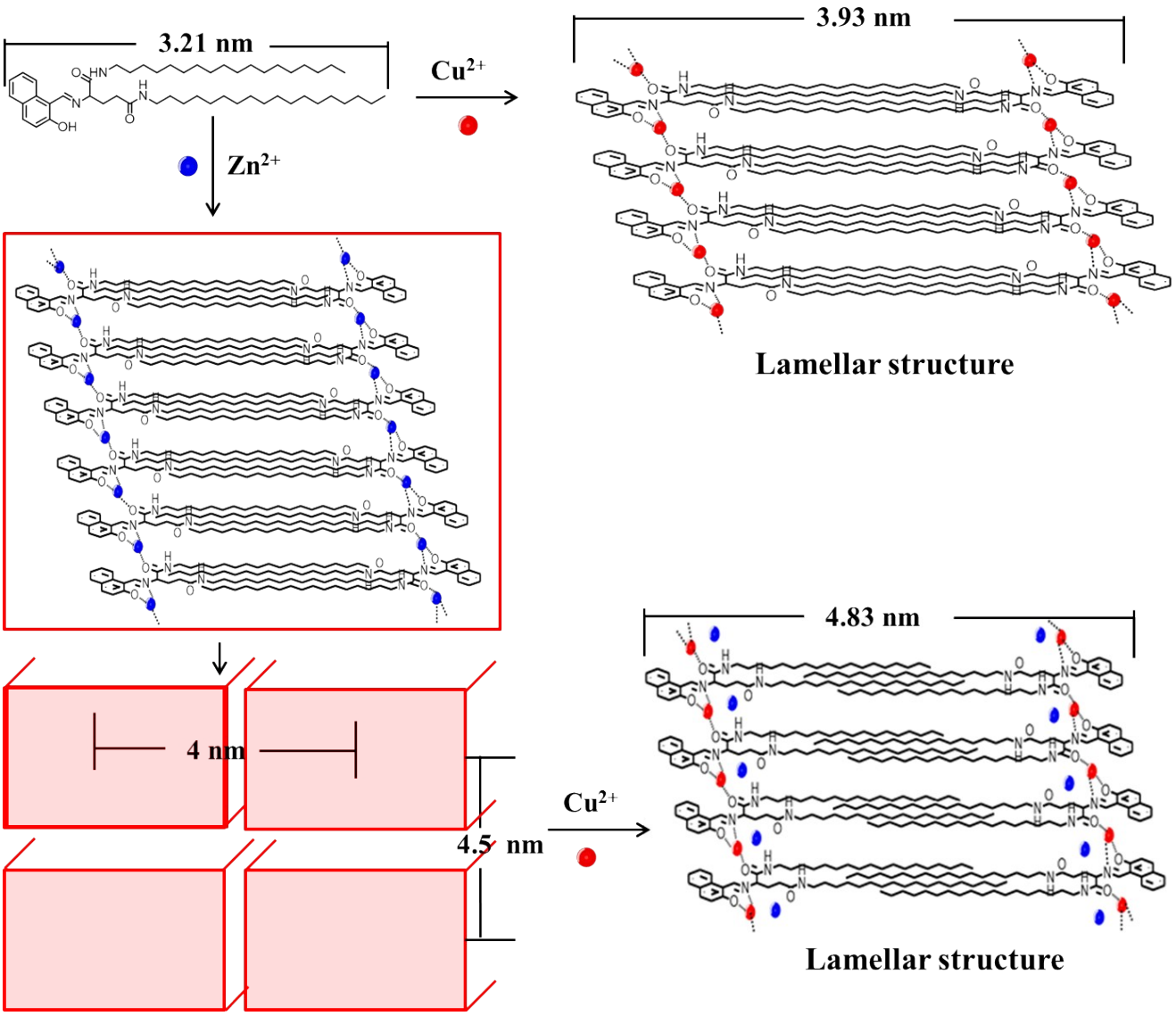

Fig. S16 Cartoon representation of the self-assembly of **CuG**, **ZnG** and **Zn-CuG.**

3. Characterization of G

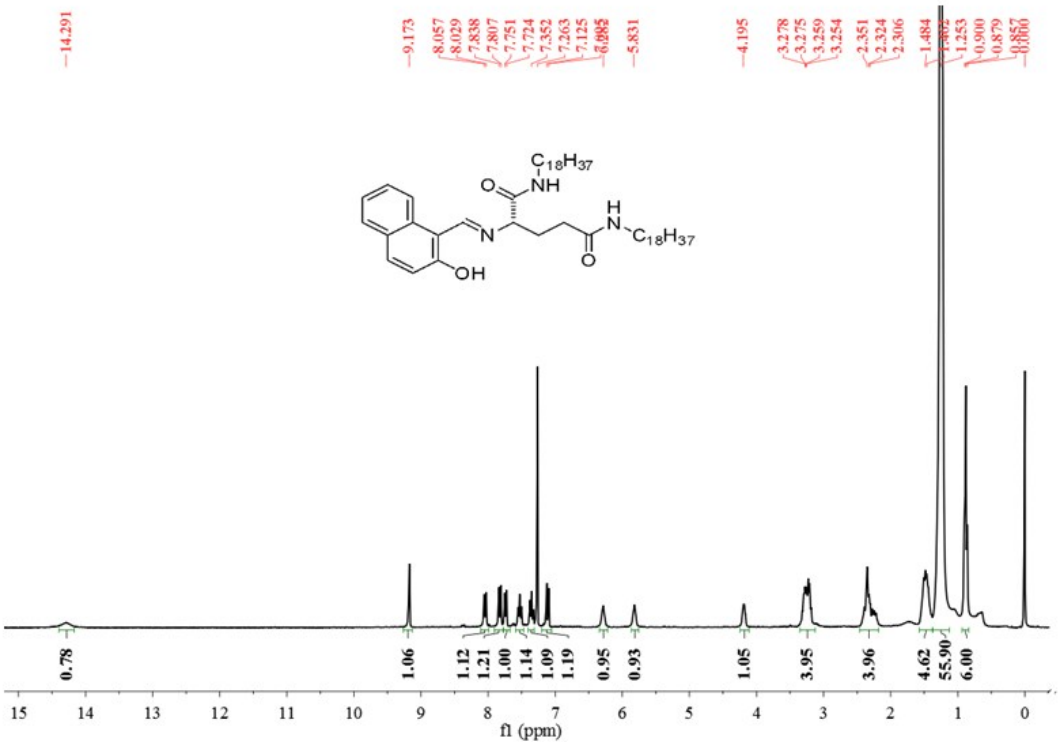

Fig. S17 ^{1}H NMR of **G**

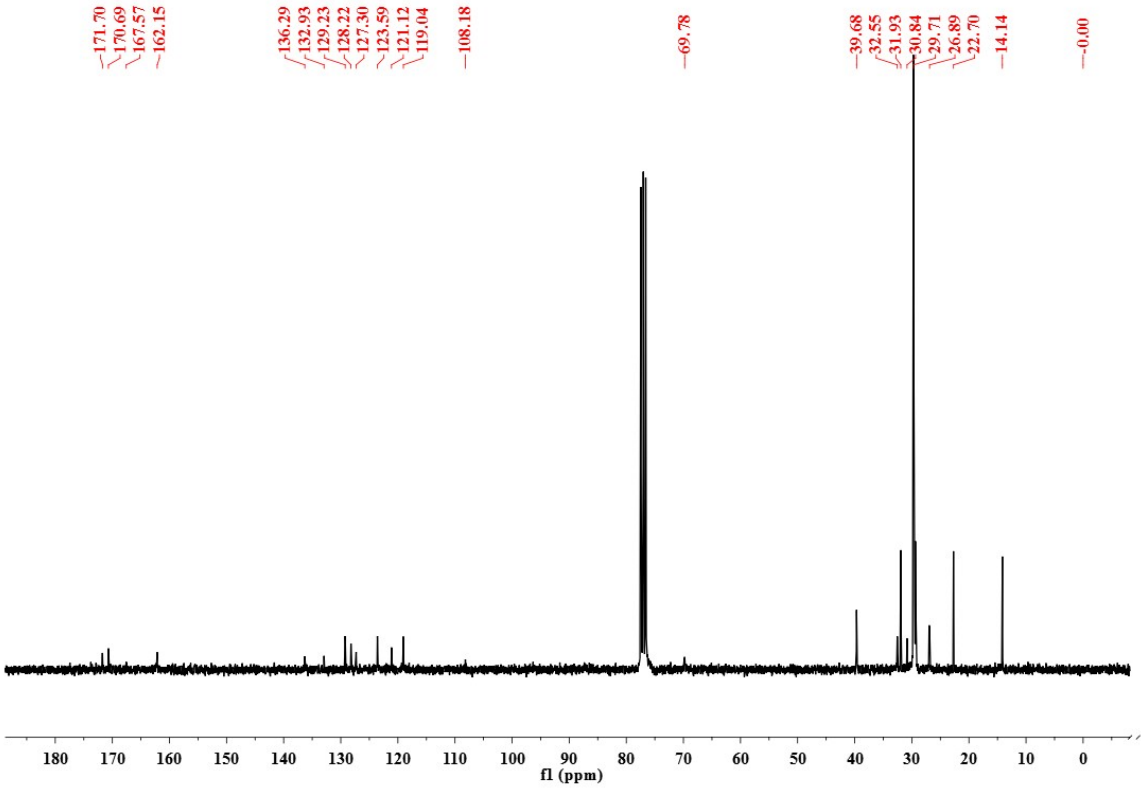

Fig. S18 ^{13}C NMR of **G**

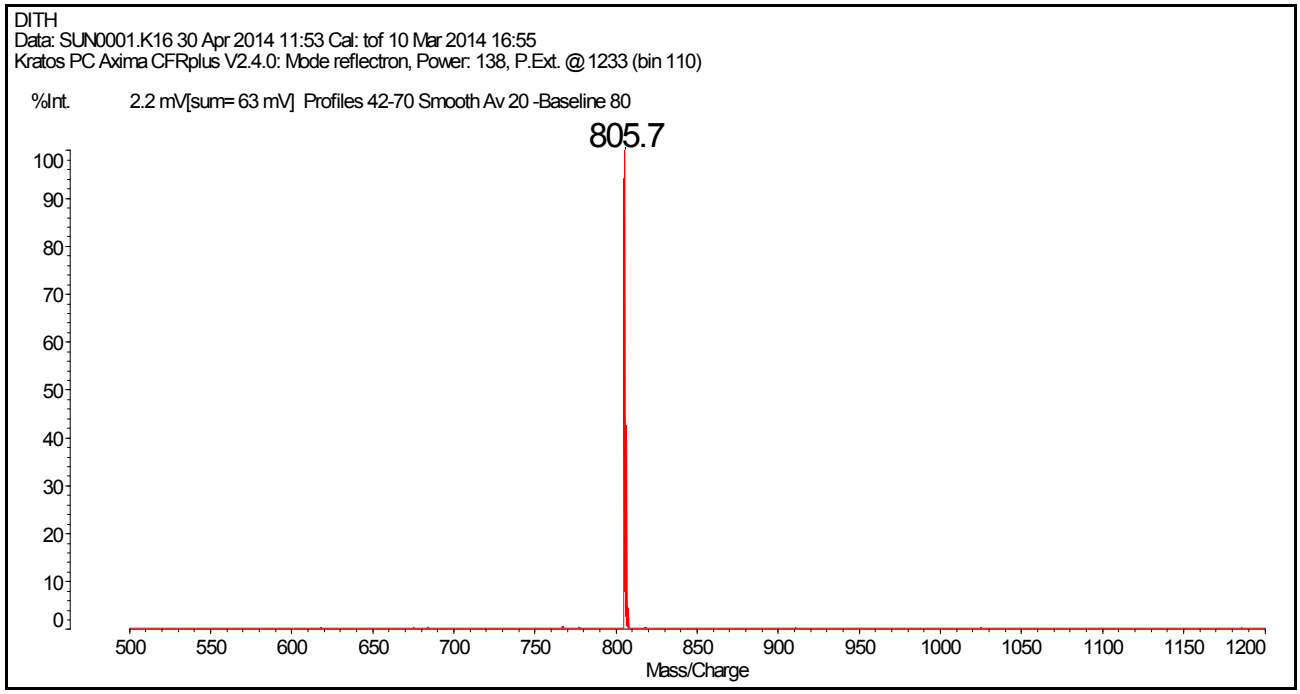

Fig. S19 MALDI-TOF-MS of **G**